Pump Characteristic Based Optimization of a Direct Water Cooling System for a 10-kW/500-kHz Vienna Rectifier

Uwe Drofenik, *Member, IEEE*, Gerold Laimer, *Student Member, IEEE*, and Johann W. Kolar, *Senior Member, IEEE*

***Abstract*—An ultra high power density 10-kW/500-kHz three-phase pulse-width modulation rectifier (Vienna Rectifier) is under development at the Power Electronic Systems Laboratory, ETH Zurich. From preliminary measurements and numerical simulations the total efficiency is assumed to be 95% at full load, resulting in power losses of up to 150 W in each multichip power module that realizes a bridge leg of the rectifier. In order to maintain the required power density of the system high direct water cooling is employed where water is in direct contact with the module base plate. Based on the measured characteristic of the water pump (pressure drop dependent on the water flow rate) the geometry of different water channel structures below the module base plate is systematically optimized based on equations which are formulated using well-established fluid dynamics theory. The design optimization is constrained by the desire to keep the geometry of the water channels in a range which allows simple and low-cost manufacturing. The aim is to find a channel structure resulting in a minimum thermal resistance of the power module for a given pump characteristic.**

In this paper, a very simple slot channel is investigated. The dependency of the thermal resistance on the cooling system is calculated for various heights of the slot channel, and an optimized channel height is determined using the condition of simple manufacturability. The shortcomings of the simple slot structure are discussed, and a novel metallic inlay structure is introduced and optimized that results in a reduction of the thermal resistance of the direct water cooling scheme as compared to the slot channel system. All theoretical considerations are experimentally verified. The general optimization scheme introduced in this paper can easily be adapted to other cooling problems.

***Index Terms*—Fluid dynamics, multichip power module, pulse-width modulation (PWM), Vienna Rectifier.**

I. Introduction

A 10-kW Vienna rectifier [1] is under development at the Power Electronic Systems Laboratory where each bridge leg is realized by a multichip power module (described in detail in [2]) employing CoolMOS switches and SiC Schottky diodes, which facilitate switching frequencies up to 500 kHz in hard-switching mode. Based on initial measurements and simulations the total system efficiency is approximately 95% and/or the power loss of each module is about 150 W. Due to the high switching frequency the inductive components can be realized in compact and light-weight form. Therefore, the volume of the heat sink and cooling system makes a significant impact on the total rectifier power density projected to be in the range of 10 kW/dm^3.

Water cooling is highly efficient in removing large quantities of heat and requires only little space compared to conventional forced air cooling. For mounting the module on a metal heat sink thermal grease is used to eliminate thin air layers which would cause thermal isolation. However, thermal grease still shows a significant thermal resistance which is often not well defined. Therefore, direct water cooling, where the water is in direct contact with the power module base plate is considered which also allows avoiding large metal heat sinks.

In this paper, a simple slot channel geometry is compared to an advanced mini-channel scheme for the following conditions.

1) Both cooling schemes are driven by pumps of equal characteristics. This condition is an important consideration in this paper.
2) Both cooling schemes are limited to the same overall dimensions.
3) Both schemes are optimized concerning minimum thermal resistance between the cooling water and the power module base plate.
4) Manufacturing of the geometry should be possible in a simple and inexpensive way. This means that microchannel structures with channel diameters of less than 100 μm are not considered.
5) The comparison is based on analytical equations and verified via numerical simulations and experimental measurements, i.e., the optimization procedure is systematic and not on a try-and-error basis.

II. Simple Slot Channel

A. Pump Characteristic and Slot Channel Geometry

A pump is generally described by a characteristic showing the pressure drop Δp_{PUMP} [N/m^2] dependent on the flow rate $\dot{v}$ [m^3/s] of the water. A heat exchanger and pipes carrying the water contribute to additional pressure drops in the cooling system. Therefore, the pressure drop Δp_{12} is measured directly across a valve which will be replaced by the heat sink later [cf. Fig. 1(a) and (b)]. The pressure drop Δp_{12} [N/m^2] is used as basis for all calculations in the following and is approximated by a second order polynomial (dimension of $\dot{v}$ is [m^3/s]) as

$$\Delta p_{12} = \Delta p_{12}(\dot{v}) = p_1 - p_2 = 14.7 \cdot 10^3 - 148.3 \cdot 10^6(\dot{v}) - 13.88 \cdot 10^{12}(\dot{v})^2. \quad (1)$$

Manuscript received March 1, 2004; revised October 5, 2004. Recommended by Associate Editor J. A. Ferreira.

The authors are with the Power Electronic Systems Laboratory, ETH Zurich, Zurich CH-8092, Switzerland (e-mail: drofenik@lem.ee.ethz.ch).

Digital Object Identifier 10.1109/TPEL.2005.846529

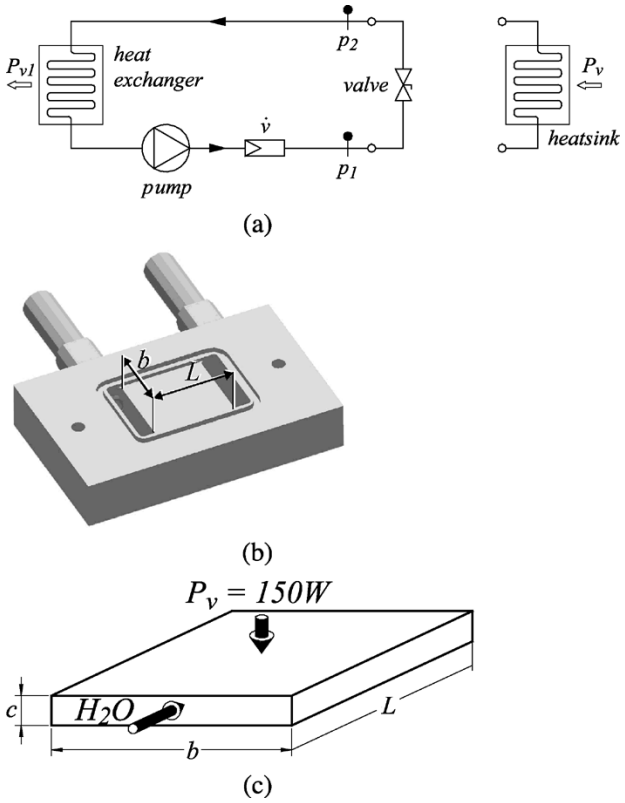

Fig. 1. (a) Cooling system employing pump, heat exchanger, and pipes. The valve is used to control the water flow while measuring the according pressure drop $\Delta p_{12} = p_1 - p_2$ for determining the characteristic of the water cooling system [cf. (1)]. After the characteristic has been determined the valve is replaced by the heat sink. (b) The heat sink is made from plastic (characterized by $\lambda_{th} = 0.25$ W/(Km)). The base plate of the power module (not shown) sitting on top of the heat sink is covering the rectangular area $A_{\mathrm{BasePlate}} = b \cdot L$ resulting in direct contact of the water with the base plate ("direct water cooling"). (c) Geometry of the slot channel carrying the water ($L = 20$ mm, $b = 19.2$ mm). Heat flow $P_V = 150$ W is impressed by the base plate of the power module.

Finding the characteristic (1) for a given cooling system is done experimentally by replacing the heat sink with a simple valve and measuring the pressure drop and the flow rate for different valve-settings. We want to point out that this measured characteristic can be very different from the pump characteristic given by the manufacturer. The pressure drop characteristic (1) is based on measurements employing a centrifugal pump *Eheim* 1048 [3] as discussed in more detail in Section II-E.

B. Calculation of Water Flow and Pressure Drop in a Slot Channel

Laminar water flow through a channel ($c \ll b$) results in a pressure drop

$$\Delta p_{\mathrm{SlotChannel,lam}}(\dot{v}) = \frac{48\rho\nu L}{(bc)d_h^2}\dot{v} \tag{2}$$

where a correction factor for slot channels as described in (6.91), (6.92) in [4] in combination with equation (3.221) given in [5] is included. In (2), $d_h = 2bc/(b+c)$ defines the hydrodynamic diameter, $\dot{v}$ [m^3/s] is the water flow, $\rho = \rho_{H20} = 992$ kg/m^3 the water density, and $\nu = \nu_{H20,40^\circ\mathrm{C}} = 658 \cdot 10^{-9}$ m^2/s the cinematic viscosity. The slot channel geometry is defined by $L = 20$ mm, $b = 19.2$ mm, where c is the optimization parameter [Fig. 1(c)]. For turbulent water flow the pressure drop in the same slot channel is determined by [(3.261) in [5]]

$$\Delta p_{\mathrm{SlotChannel,turb}}(\dot{v}) = \frac{L\frac{b+c}{2bc}\rho\frac{1}{2}\left(\frac{\dot{v}}{bc}\right)^2}{\left(0.79 \cdot \ln\left(\frac{2\dot{v}}{(b+c)\nu}\right) - 1.64\right)^2}. \tag{3}$$

For determining if the water flow is laminar or turbulent one has to calculate the Reynolds number

$$Re_{\mathrm{Channel}} = \frac{w_m \cdot d_h}{\nu} = \frac{2\dot{v}}{(b+c)\nu} \tag{4}$$

of the problem (p. 351 in [5]) with the average flow velocity

$$w_m = \frac{\dot{v}}{A_q} = \frac{\dot{v}}{(bc)}. \tag{5}$$

For $Re_{\mathrm{Channel}} < 2300$ the problem is laminar [(7.1) in [4]], otherwise is turbulent. Assuming the problem as turbulent, the water flow $\dot{v}$ for a given geometry (L, b, c) of the slot channel can be calculated using (1) and (3). Based on $\dot{v}$, one can then calculate the Reynolds number employing (4). If the Reynolds number is higher than 2300 the assumption is justified, otherwise the water flow $\dot{v}$ and the Reynolds number have to be calculated using (1) and (2). This mathematical procedure is shown in Fig. 2 for different values of the channel height c. Water flow, pressure drop and Re_{Channel} are shown in Fig. 3 with dependency on the height c of the slot channel (see Fig. 1(c) for geometry-definitions). For small heights, c, the pressure drop across the heat sink increases significantly and the water flow is reduced accordingly. Only for very small channel heights ($c < 250\ \mu$m) is the flow laminar.

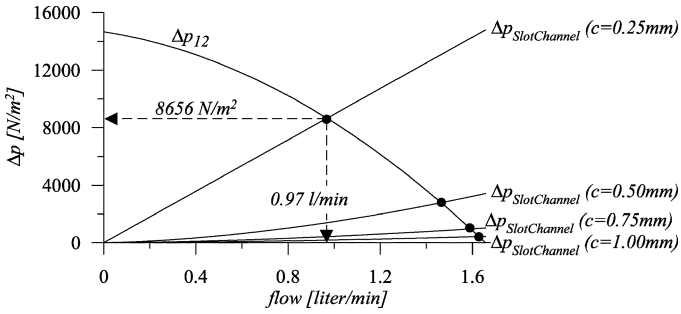

Fig. 2. Pump characteristic $\Delta p_{12}(\dot{v})$ and heat sink characteristic $\Delta p_{\mathrm{SlotChannel}}(\dot{v})$ defining the actual water flow $\dot{v}$ and the pressure drop Δp [N/m^2] for a selected slot channel geometry ($L = 20$ mm, $b = 19.2$ mm). Note that the water flow $\dot{v}$ is given in all diagrams in [l/min] while all calculations including (1) are performed in SI-units [m^3/s].

C. Calculation and Minimization of the Thermal Resistance of the Slot Channel Geometry

Since the heat sink only has to guide the water flow and does not have to conduct heat it can be made of plastic. The heat flow is directly from one wall, i.e., the power module base plate into the water. Therefore, the thermal model for water flow along a hot plate has to be applied. With the average flow velocity w_m

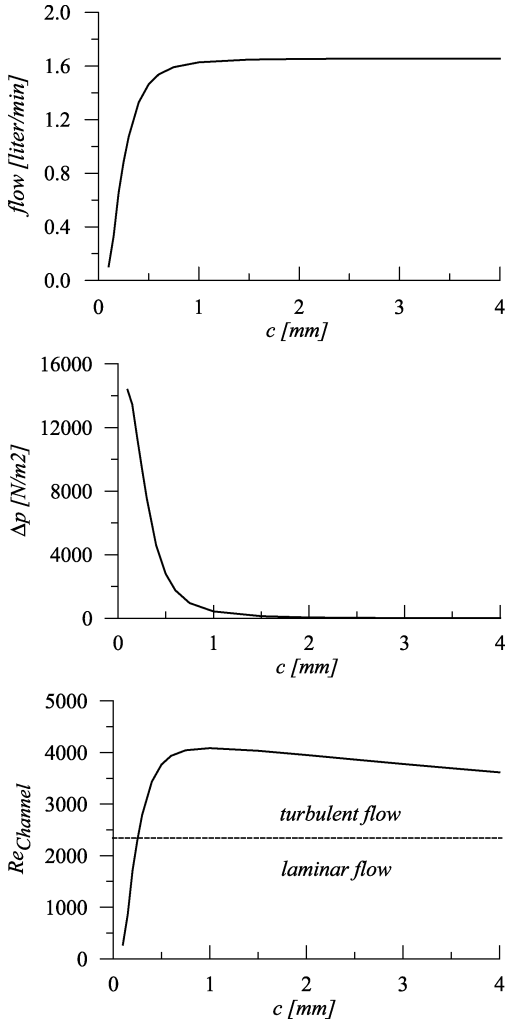

Fig. 3. Water flow, pressure drop (cf. Fig. 2) and Reynolds number indicating laminar or turbulent flow in dependency of the slot channel geometry (height c).

already calculated in (5), this type of thermal problem comes with a different definition (p. 324 in [5]) of the Reynolds number

$$Re_{\mathrm{AlongPlate}} = \frac{w_m \cdot L}{\nu}. \tag{6}$$

For calculating the thermal resistance we first have to define the Nusselt number, $Nu_{\mathrm{AlongPlate}}$, which is defined for this type of problem, equally valid for laminar and turbulent flow, as given by equations (3.196), (3.207), (3.208) in [5] and/or (11), (12) in [6]) as (7) shown at the bottom of the page.

In [6], the accuracy of (7) is given as $\pm 20\%$ compared to experimental data over a very wide parameter range. According to (6) we find for the parameter range of this paper $10\,000 < Re_{\mathrm{AlongPlate}} < 100\,000$ results in a maximum error of $\pm 15\%$ (see Fig.2 in [6] and/or experimental data in [7]). The boundary flow conditions at the inlet of the slot channel are described by the fluid velocity vector-field which will be highly nonuniform in case of a nonidealized technical system (discussed in Section II-D). The main impact of the flow boundary condition at the channel inlet is on the value of the critical Reynolds number which determines if the flow is laminar or turbulent. The critical value of $Re_{\mathrm{critical}} = 2300$, as given in the previous section and used throughout this paper, is valid for typical technical applications while the (2) and (3) are not affected by the inflow conditions.

The Prandtl number, Pr in (7), is a fluid parameter, for water we have $Pr = Pr_{H20,40\,^\circ\mathrm{C}} = 4.328$. Based on $Nu_{\mathrm{AlongPlate}}$ one can calculate the thermal resistance $R_{\mathrm{th,aboveSlot}}$ between the water [$T_a = T_{\mathrm{H20,ambient}} = 40\,^\circ\mathrm{C}$, $\lambda_{H20} = 0.63\,\mathrm{W/(Km)}$] and the base plate above the slot channel as [(1.47) and (1.77) in [5]]

$$\begin{aligned} R_{\mathrm{th,aboveSlot}} &= \frac{L}{Nu_{\mathrm{AlongPlate}} \lambda_{H20} A_{\mathrm{BasePlate}}} \\ &= \frac{1}{Nu_{\mathrm{AlongPlate}} \lambda_{H20} b}. \end{aligned} \tag{8}$$

As shown in Fig. 4, the minimum thermal resistance $R_{\mathrm{th,MIN}} = 0.1$ K/W results for $c = 300\ \mu$m. This is in accordance with the theory of micro-channels for single-phase liquid cooling systems ([8]).

D. Influence of the Pipe Structure Between Water Inlet/Outlet of the Heat Sink and the Slot Channel

1) Additional Pressure Drop: In the previous Sections II-B and II-Cthe thermal resistance between base plate and water in the slot channel has been discussed resulting in Fig. 4(a). The influence of the pipe structure inside the heat sink guiding the water between inlet/outlet and slot channel has been neglected. The pipe structure influences all calculations due to an additional internal pressure drop and additional heat transfer between base plate and water across the inflow area and the outflow area where the slot channel geometry cannot be applied. Fig. 5 shows details of the three-dimensional (3-D) pipe structure.

Analytical equations describing the pressure drop in all kinds of pipes of circular and noncircular cross-sections along different kinds of bends are given in the literature in the very general form (based on experiments)

$$\Delta p = \xi \cdot \frac{\rho}{2} w_m^2 \tag{9}$$

with values of the coefficient ξ given in tables (e.g., p. B52 in [9]). A straightforward calculation of the total pressure drop in the pipe structure defines all relevant values of ξ along the water flow path shown by the solid line in Fig. 5. The according flow velocities w_m are given by the quotient of water flow rate $\dot{v}$ and

$$Nu_{\mathrm{AlongPlate}} = \sqrt{\left[\frac{2 \cdot \frac{\sqrt{\pi}}{2} Re_{\mathrm{AlongPlate}}^{\frac{1}{2}} Pr^{\frac{1}{2}}}{\left(1 + 2.09 \cdot Pr^{\frac{1}{4}} + 48.74 \cdot Pr\right)^{\frac{1}{6}}}\right]^2 + \left[\frac{0.037 \cdot Re_{\mathrm{AlongPlate}}^{0.8} Pr}{1 + 2.443 \cdot Re_{\mathrm{AlongPlate}}^{-0.1}\left(Pr^{\frac{2}{3}} - 1\right)}\right]^2}. \tag{7}$$

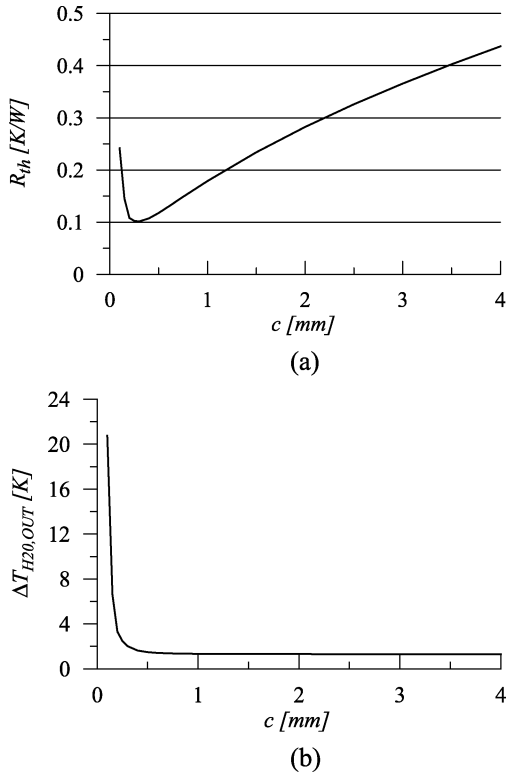

Fig. 4. (a) Thermal resistance, between the power module base plate above the slot channel (area $L \cdot b$) and cooling water, dependency on the channel height c [cf. Fig. 1(c)]. (b) Difference ΔT of water temperature between entrance and end of the slot channel for various channel heights. For narrow channels (small values of c) ΔT increases as the water flow reduces [Fig. 3(a)], resulting in a sharp increase of the thermal resistance.

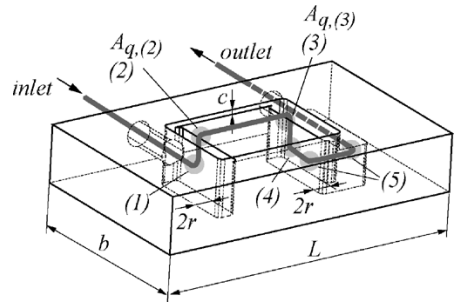

Fig. 5. Geometry of the 3-D pipe structure inside the heat sink guiding the water flow along inlet → inflow area → slot channel (height c) → outflow area → outlet. The gray shaded regions labeled (1), (2), (3), (4), (5) indicate locations of significant pressure drop within the pipe structure.

the actual cross sectional area A_q. Adding all individual pressure drops results in a total pressure drop of the given pipe structure $\Delta p_{\mathrm{PipeStructure}}$. In consideration of the fact that pipe bends show a significant contribution to the pressure drop, the locations of large pressure drops are highlighted in gray and labeled as (1)...(5) in Fig. 5. Unfortunately, the ξ-values of bends vary by a factor of eight according to the exact definition of pipe and bend. For the complex 3-D flow pattern within the pipe structure it is, therefore, not possible to accurately calculate the pressure drop $\Delta p_{\mathrm{PipeStructure}}$ without any experimental measurements or numerical CFD-simulations.

We can write in a very general form

$$\Delta p_{\mathrm{PipeStructure}} = \sum_{i=1\ldots5} \xi_{(i)} \cdot \frac{\rho}{2} w_{m,(i)}^2 = \frac{\rho}{2}\dot{v}^2 \sum_{i=1\ldots5} \frac{\xi_{(i)}}{A_{q,(i)}^2}. \tag{10}$$

The water flow cross sectional areas $A_{q,(2)}$ and $A_{q,(3)}$ [at bends (2) and (3)] are proportional to the slot channel cross-sectional area $A_{\mathrm{q,SlotChannel}} = b \cdot c$ as shown in Fig. 5. Therefore, (10) can be written generally as

$$\begin{aligned}\Delta p_{\mathrm{PipeStructure}} &= \frac{\rho}{2}\dot{v}^2 \left(\frac{\xi_{(1)}}{A_{q,(1)}^2} + \frac{\xi_{(2)}}{A_{q,(2)}^2} + \frac{\xi_{(3)}}{A_{q,(3)}^2} + \frac{\xi_{(4)}}{A_{q,(4)}^2} + \frac{\xi_{(5)}}{A_{q,(5)}^2} \right) \\ &= \left(x_a + \frac{x_b}{A_{\mathrm{q,SlotChannel}}^2} \right) \dot{v}^2. \end{aligned} \tag{11}$$

The parameters x_a and x_b are to be defined experimentally. This means that two heat sinks with different slot channel heights c have to be manufactured and the corresponding flow rates $\dot{v}$ and pressure drops Δp_{12} have to be measured. Equations (2) and (3) have to be modified as

$$\begin{aligned}\Delta p_{12,lam}(\dot{v}) &= \Delta p_{\mathrm{SlotChannel,lam}}(\dot{v}) \\ &\quad + \left(x_a + \frac{x_b}{A_{\mathrm{q,SlotChannel}}^2} \right) \dot{v}^2 \end{aligned} \tag{12}$$

$$\begin{aligned}\Delta p_{12,turb}(\dot{v}) &= \Delta p_{\mathrm{SlotChannel,turb}}(\dot{v}) \\ &\quad + \left(x_a + \frac{x_b}{A_{\mathrm{q,SlotChannel}}^2} \right) \dot{v}^2. \end{aligned} \tag{13}$$

Inserting the two measured flow rates and pressure drops with value of c in (12) and (13), and defining the flow type dependent on the Reynolds-number [(4) and (5)] gives two equations for x_a and x_b. For two different slot channel heat sinks with $c =$ 0.35 mm and $c = 2.5$ mm we obtained experimentally $x_a =$ 8.3e12 and $x_b = 130$. This is valid in good approximation for all channel geometries discussed in this paper because the pipe structure is not changed.

2) Thermal Resistance of Inflow/Outflow Area: Not only does the heat flow from the base plate into the water but also the inflow area and the outflow area contribute to the thermal resistances $R_{\mathrm{th,IN}}$ and $R_{\mathrm{th,OUT}}$, and are connected in parallel to the thermal resistance of the channel (Fig. 4). The water flow in these two areas is complex to describe analytically and specific for the problem, therefore no such models are available in the literature. Based on CFD-simulations we found a good approximation of $R_{\mathrm{th,flowArea}} = R_{\mathrm{th,IN}} \| R_{\mathrm{th,OUT}} = 0.4$ K/W for $c > 1.2$ mm and $R_{\mathrm{th,flowArea}} = R_{\mathrm{th,IN}} \| R_{\mathrm{th,OUT}} = 1.0$ K/W for $c < 1.2$ mm. This rough approximation is justified because the thermal resistance of the channel area at its minimum is significantly smaller than $R_{\mathrm{th,flowArea}}$. The definition of $R_{\mathrm{th,flowArea}}$ is not dependent on the channel geometry and can, therefore, in good approximation be employed for all cooling schemes discussed in this paper.

E. Experimental Results

The experimental setup shown in Fig. 1(a) comprises of a centrifugal pump (*Eheim* 1048 [3]), a heat exchanger, and pipes with circular cross sectional area and an inner diameter of 8 mm. The heat sink is manufactured from PEEK polymer material which is convenient for rapidly producing prototypes by cutting and milling. For mass production one would, alternatively, employ, e.g., POCAN which could be manufactured in a cost-efficient way by injection molding. Heat sinks with slot channel heights $c = 0.2$ mm, 0.35 mm, 0.75 mm, 1.5 mm, and 2.5 mm have been manufactured. The power module was replaced by a heat source made by a block of copper with heating resistors placed on top. This heat source is thermally isolated so that all heat flows directly from the heating resistors through the copper block to the water surface (Fig. 6). The copper block acts as a heat spreader creating equally distributed thermal power flow

$$\dot{q} = \frac{P_V}{A_{\mathrm{BasePlate}}} = \frac{150\ \mathrm{W}}{25 \cdot 34\ \mathrm{mm}^2} = 17.6\ \frac{\mathrm{W}}{\mathrm{cm}^2} \qquad (14)$$

into the water. The "base-plate" temperature is measured by K-type thermocouples (accuracy 2%, see [10]) put into two holes (2-mm diameter) of the copper block located as shown in Fig. 6. Since the thermal conductivity of copper is not infinite, there is a small temperature gradient along the base plate of $\Delta T < 4\,^{\circ}\mathrm{C}$ for $c < 2.5$ mm which is influenced by the location of the heating resistors but especially by the water flow direction since the water is heating up by about 2.0 °C from inlet to outlet [see Fig. 4(b)]. The temperature of the cooling water is 30 °C at the inlet. For calculating the thermal resistance of the cooling system the average value of the two measured temperatures is formed. CFD-simulations with ICEPAK [11] have shown that the average temperature measured in this way is in agreement within less than 6% of the numerically calculated average temperature distribution over the base plate.

The pressure drop Δp_{12} according to (1) is measured with a differential pressure sensor *XFDM-025KPDSR* (accuracy $\pm 2\%$, see [12]) connected in parallel to the inlet/outlet of the heat sink. The water flow is measured by a sensor [13] located as shown in Fig. 1(a). The measurement results depicted in Fig. 7 show a good match with the theoretical predictions (solid lines, considering (12), (13), [Section II-D-2)]. The dashed lines show the theory neglecting the influence of the internal pipe structure of the heat sink (see Sections II-B and II-C). Only in close vicinity of the minimum of the thermal resistance R_{th} (Fig. 4) the additional parallel thermal resistance $R_{\mathrm{th,flowArea}}$ can be neglected.

III. Improving the Simple Slot Channel by a Novel Metal Inlay Concept

A. Metal Inlay Concept

The main idea of the slot channel described in the previous section is to bring the base plate of the power module in direct contact with the water in order to avoid thermal resistances which would be introduced by a thermal grease layer between base plate and a conventional metal heat sink. The main disadvantage of the slot channel structure is that the surface injecting heat into the cooling medium is limited to the base plate area.

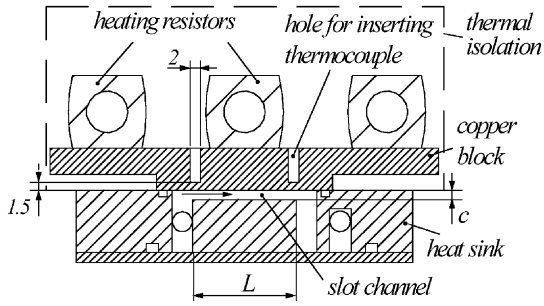

Fig. 6. Thermally isolated copper block with heating resistors and thermocouples replacing the power module and providing equally distributed thermal power flow of 17.6 W/cm^2.

Fig. 8 shows a novel concept employing a metal inlay which is positioned directly below the base plate of the power module and provides a mini-channel structure for the water flow. A rubber-ring inserted between inlay and plastic heat sink provides a spring force and ensures direct contact of the inlay fins and the base plate metal surface. The gap between the inlay fins and the base plate is not filled with air $[\lambda_{\mathrm{AIR}} = 0.026\ \mathrm{W/(Km)}]$ and/or thermal grease (typically $\lambda_{\mathrm{GRASE}} \approx 0.4 \ldots 1.0\ \mathrm{W/(Km)}$) but with water $(\lambda_{H20} = 0.630\ \mathrm{W/(Km)})$ which results in a significant reduction of the thermal resistance. The heat is flowing from the base plate partly directly into the water, and partly into the fins which effectively increases the cooling surface and results in a significant reduction of the thermal resistance. In the following, the inlay geometry will be optimized for minimum thermal resistance. The geometry of the inlay-channels is characterized by

$$k = \frac{b_{MI}}{\frac{b}{n}}. \qquad (15)$$

Remark: The inlay-concept is advantageous only if the thermal resistance of the nonmoving water layer $d_{\mathrm{interface}}$ in the gap between base plate and inlay fins is smaller than the thermal resistance of the simple slot channel. If this condition is violated the thermal resistance will always be higher than for the slot channel. Fig. 9 shows, that for the system under investigation (pump characteristic as given in (1), geometry of the power module base plate 3.4×2.5 cm^2) the condition $R'_{\mathrm{th,H20}} < R'_{\mathrm{th,SlotChannel}}$ is fulfilled. The thickness of the interface $d_{\mathrm{interface}}$ is assumed to be about 1 μm due to the surface roughness of the base plate and the inlay fins measured using a microscope. The power module [2] in this paper uses a DBC without heat-spreading copper base plate (220 μm Si-Chips—300 μm Cu layout—630 μm Al_2O_3 ceramic isolator—300 μm Cu bottom layer). It, therefore, does not show a bow which is typical for many power modules with copper base plate heat spreader, and can be assumed as flat.

B. Calculation of Water Flow and Pressure Drop

Defining the hydraulic diameter $d_h = 2b_{MI}c/(b_{MI} + c)$ for the geometry given in Fig. 8(c) the water flow through the inlay

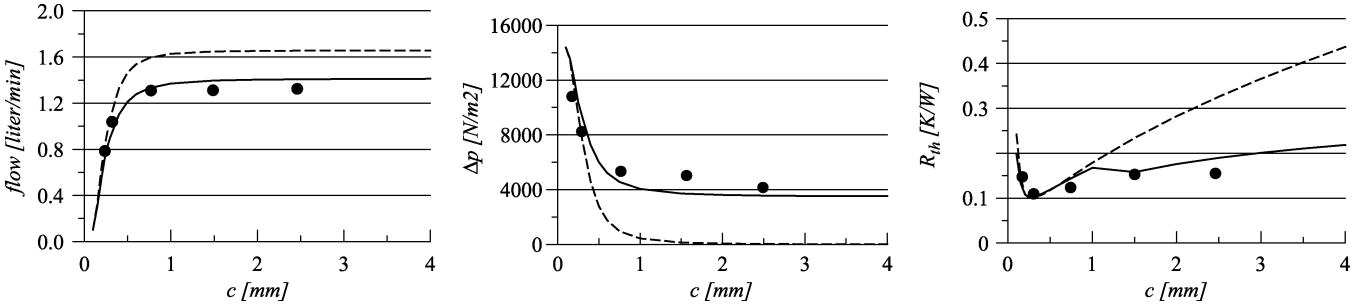

Fig. 7. Neglecting the influence of the pipe structure inside the heat sink results in the characteristics shown by dashed lines [already shown in Fig. 3 and Fig. 4(a)]. Performing the calculations as described in Section II-D gives the curves shown by solid lines. Results of experimental measurements are indicated by black dots.

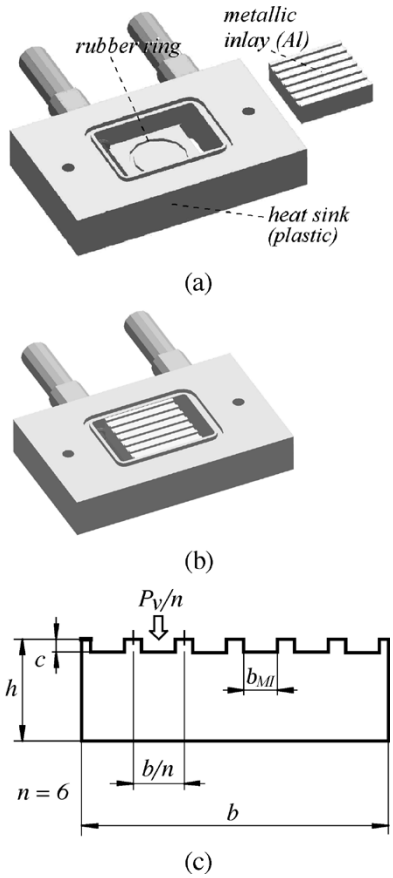

Fig. 8. Novel metallic inlay concept shown (a) separated from the plastic heat sink and (b) assembled. (c) Geometry of metal inlay ($h = 6$ mm, $b = 19.2$ mm).

channels creates a pressure drop across the heat sink which is given for laminar flow as [(3.221) in [5]]

$$\Delta p_{\mathrm{Inlay,lam}}(\dot{v}) = \frac{32\rho\nu L}{n(b_{MI}c)d_h^2}\dot{v} \tag{16}$$

where n is the number of channels. For turbulent flow the pressure drop is given as [(3.261) in [5]]

$$\Delta p_{\mathrm{Inlay,turb}}(\dot{v}) = \frac{L\frac{b_{MI}+c}{2b_{MI}c}\rho\frac{1}{2}\left(\frac{\dot{v}}{n(b_{MI}c)}\right)^2}{\left(0.79\cdot\ln\left(\frac{2\dot{v}}{n(b_{MI}+c)\nu}\right)-1.64\right)^2} \tag{17}$$

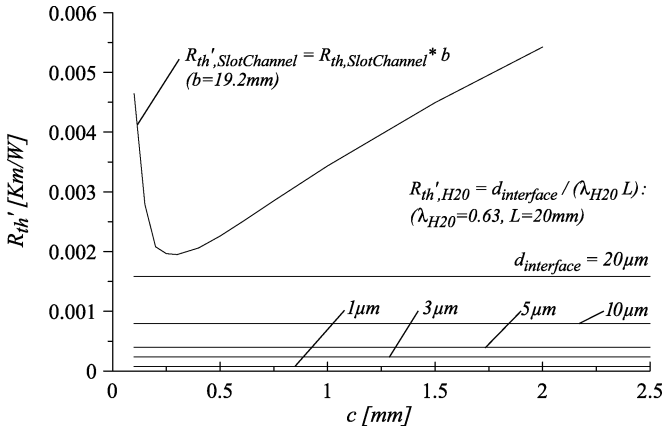

Fig. 9. Comparison of the normalized thermal resistance of the simple slot channel ($R'_{\mathrm{th,SlotChannel}}$) and normalized thermal resistance of an interface layer consisting of nonmoving water ($R'_{\mathrm{th,H20}}$) as present between the base plate and the fins of the metal inlay.

with the Reynolds number defined for this problem as (page 351 in [5])

$$Re_{\mathrm{InlayChannel}} = \frac{w_m\cdot d_h}{\nu} = \frac{2\dot{v}}{n(b_{MI}+c)\nu} \tag{18}$$

indicating laminar flow (for $Re_{\mathrm{InlayChannel}} < 2300$) or turbulent flow. Proceeding in analogy to Section II-B water flow and pressure drop for certain geometries of the inlay channel structure can be calculated as shown in Fig. 10 where pump, pipes and heat exchanger are included based on the measured characteristic (1).

C. Calculation of the Thermal Resistance of the Power Module Base Plate

With the definition of the Reynolds number (18) the Nusselt number $Nu_{\mathrm{InlayChannel,lam}}$ can be calculated for laminar flow ($Re_{\mathrm{InlayChannel}} < 2300$) as [(3.250), (3.255) in [5]]

$$Nu_{\mathrm{InlayChannel,lam}} = \frac{3.657\left[\tanh\left(2.264X^{\frac{1}{3}}+1.7X^{\frac{2}{3}}\right)\right]^{-1}+\frac{0.0499}{X}\tanh(X)}{\tanh\left[2.432\,\mathrm{Pr}^{\frac{1}{6}}X^{\frac{1}{6}}\right]} \tag{19}$$

with

$$X = \frac{L}{d_h Re_{\mathrm{InlayChannel}} Pr} \tag{20}$$

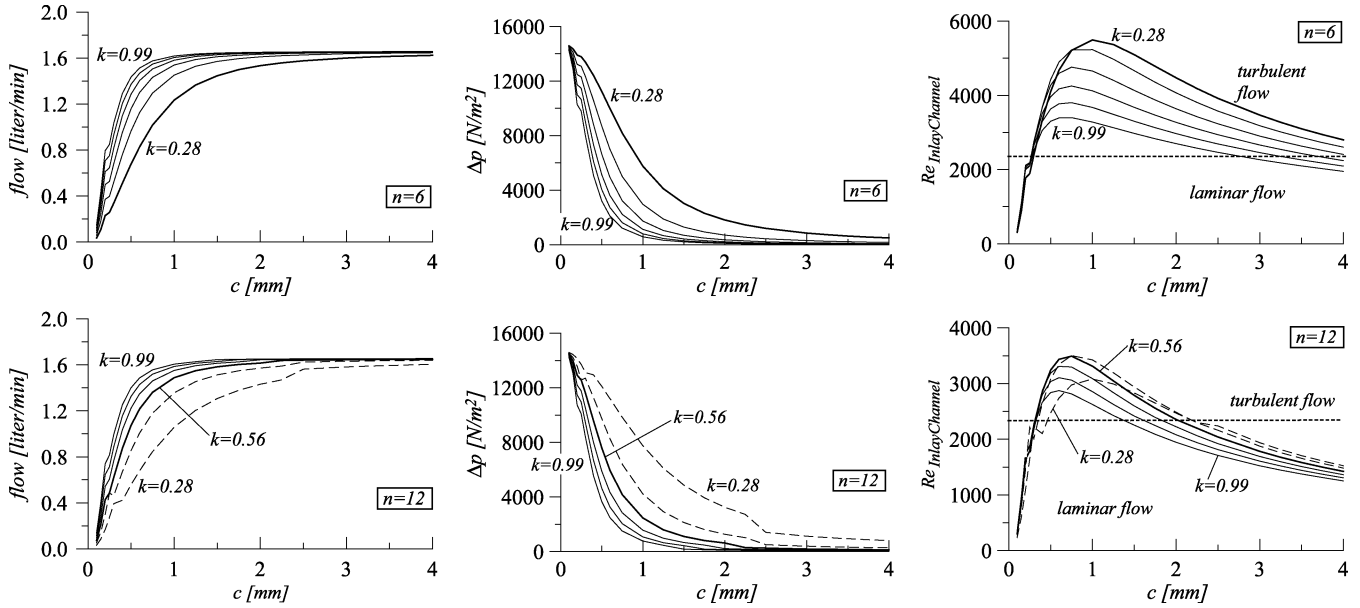

Fig. 10. Water flow, pressure drop and Reynolds number indicating laminar or turbulent flow in dependency of the inlay geometry with $n = 6$ and $n = 12$. Dashed curves indicate that the condition of easy manufacturing ($b_{MI} > 0.9$ mm) is violated. Family of curves is for channel ratios of $k = b_{MI}/(b/n) = [0.28,\ 0.42,\ 0.56,\ 0.70,\ 0.84,\ 0.99]$. The dotted horizontal line marks the border between laminar and turbulent flow at $Re_{\mathrm{InlayChannel}} = 2300$. For channel ratios $k = b_{MI}/(b/n)$ close to 1.0 (decreasing width of the fins) the cross section of the inlay $(n \cdot b_{MI}c)$ becomes equal to the cross section of the slot channel $(b \cdot c)$ but the pressure drop is different due to the mechanical friction of the fluid along the fins, which is independent from the width of the fins. Therefore, $Re_{\mathrm{InlayChannel}}$ for $k = 0.99$ changes for different channel-numbers n and is also different from Re_{Channel} in Fig. 3.

and for turbulent flow ($Re_{\mathrm{InlayChannel}} > 2300$) as [(3.260), (3.261) in [5] and/or (14) in [14]] as (21) shown at the bottom of the page.

Equation (19) provides an empirical correlation of results derived from numerical solutions of the Navier–Stokes differential equations describing flow and heat exchange in idealized pipe-models (chapter 3.8.1.5 in [5]). The accuracy between empirical correlation and numerical solution is within $\pm 5\%$ over a wide parameter range. For (17), derived in the same way, an accuracy of $\pm 1.65\%$ compared to the idealized models is given (chapter 3.8.1.5 in [5]). Equation (21) is an empirical correlation of experimental data with an accuracy of $\pm 20\%$ according to [14].

In contrast to the theory of water flow along a hot plate described by (6) and (7) in connection with the slot channel, the determination of the heat transfer problem of the inlay concept [(19)–(21)] is based on the theoretical model of rectangular channels where all walls are heated. Under the assumption of high thermal conductivity of the metallic inlay ($\lambda_{Al} = 237\ \mathrm{W/(Km)}$) this is valid with good accuracy

$$\alpha = Nu_{\mathrm{InlayChannel}} \cdot \frac{\lambda_{H20}}{d_h} \tag{22}$$

$$R_{th,H20} = \frac{d_{\mathrm{interface}}}{\left(\frac{\lambda_{H20} L\left(\frac{b}{n} - b_{MI}\right)}{2}\right)} \tag{23}$$

$$R_{th,M1} = \frac{\left(\frac{c}{2}\right)}{\left(\frac{\lambda_{Al} L\left(\frac{b}{n} - b_{MI}\right)}{2}\right)} \tag{24}$$

$$R_{th,M2} = R_{th,M1} + \frac{\left(\frac{b_{MI}}{2}\right)}{(\lambda_{Al} L(h-c))} \tag{25}$$

$$R_{th,\alpha 1} = \frac{1}{(\alpha L c)} \tag{26}$$

$$R_{th,\alpha 2} = \frac{1}{(\alpha L\, b_{MI})} \tag{27}$$

$$\begin{aligned} R_{th} &= R_{th}(d_{\mathrm{interface}}, Nu_{\mathrm{InlayChannel}}) \\ &= R_{th,\alpha 2} \| \\ &\quad \times \left[\left(\frac{1}{2} R_{th,H20} + \frac{1}{2} R_{th,M1} \right) \right. \\ &\quad \left. + \left(\frac{1}{2} R_{th,M2} + R_{th,\alpha 2} \right) \| \left(\frac{1}{2} R_{th,\alpha 1} \right) \right]. \end{aligned} \tag{28}$$

The network of thermal resistances in Fig. 11 describes the heat transfer from the power module base plate into the water for one channel. There, $R_{\mathrm{th,H20}}$ is the thermal resistance of the contact area of the fins and the base plate. For calculating the thermal resistance $R_{\mathrm{th,H20}}$ we assume a metallic surface roughness of $0.8\ \mu\mathrm{m} \ldots 1.6\ \mu\mathrm{m}$ (measured using a microscope), neglect small areas where both metal surfaces are in direct contact, and assume that the gap between both surfaces is entirely

$$Nu_{\mathrm{InlayChannel,turb}} = \frac{\left\{8 \cdot (0.79 \cdot \ln(Re_{\mathrm{InlayChannel}}) - 1.64)^2\right\}^{-1} (Re_{\mathrm{InlayChannel}} - 1000) Pr}{1 + 12.7\sqrt{\left\{8 \cdot (0.79 \cdot \ln(Re_{\mathrm{InlayChannel}}) - 1.64)^2\right\}^{-1}} \left(Pr^{\frac{2}{3}} - 1\right)} \left[1 + \left(\frac{d_h}{L}\right)^{\frac{2}{3}}\right]. \tag{21}$$

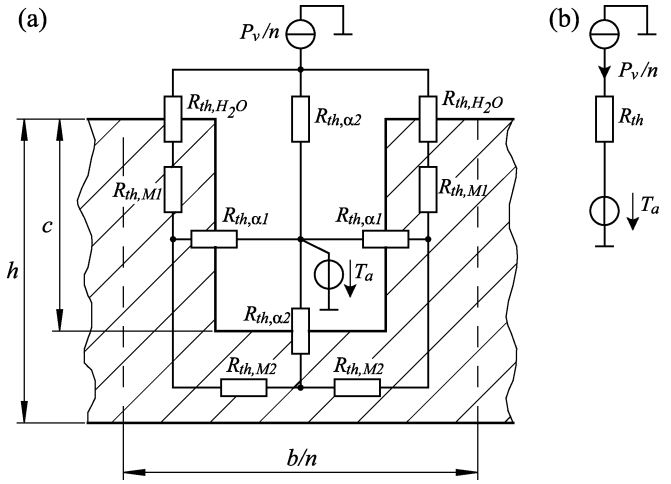

Fig. 11. (a) Thermal network describing (stationary) the heat conduction between power module base plate and water. The thermal power flow is direct ($R_{th,\alpha 2}$) and via the metal inlay. The resistance values of the thermal equivalent circuit are given in (22)–(27). (b) The network can be transformed into a single resistance R_{th} as defined in (28).

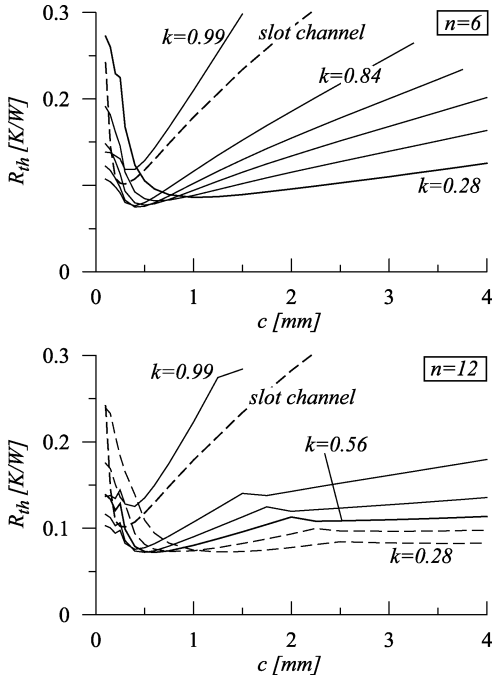

Fig. 12. Thermal resistance between power module base plate and water depending on the height c of the channel [cf. Fig. 8(c)] for different channel ratios $k = b_{MI}/(b/n)$ and $n = 6$ or $n = 12$. The curves are given for channel ratios of $k = b_{MI}/(b/n) = [0.28,\ 0.42,\ 0.56,\ 0.70,\ 0.84,\ 0.99]$..

filled with water. This contact area will be modeled as a layer of nonmoving water (no heat convection) with a thickness of $d_{\text{interface}} = 1.0\ \mu$m. The resulting thermal resistance $R_{\text{th,H20}}$ can be calculated according to (22) and (23).

In analogy to Section II-C the thermal resistance can be calculated from (16)–(28) dependent on the geometry of the inlay structure (Fig. 12). Concerning heat flow for $k = 0.99$ the influence of the fins is negligible and the inlay geometry is equal to the slot channel geometry. The curve of the slot channel [Fig. 4(a)] is shown in both diagrams as dotted line and is very close to the inlay channel curve of $k = 0.99$. As the slot channel and the metal inlay considerations are based on different theories of heat transfer, this result shows the good consistency of the theory describing the heat transfer problems in this paper. But, as discussed in the caption of Fig. 10, these two geometries are not equivalent concerning the pressure drop and the Reynolds number. Since the Nusselt number is dependent on the Reynolds number [(7), (19)–(21)] small differences between the two curves especially at higher values of c can be explained. For $n = 12$ geometries which are difficult to manufacture (condition for easy manufacturing: $k > 0.55 \rightarrow b_{MI} > 0.9$ mm) are shown by dashed lines.

D. Experimental Results

The calculations (16)–(28) resulting in the characteristics of Fig. 12 are performed neglecting the influence of the internal pipe structure of the heat sink. Since this pipe structure is unchanged, (11)–(13) can be employed using the same parameter values x_a, x_b as given in Section II-D. There, the channel cross section $A_{\text{q,SlotChannel}}$ in (11) has to be replaced with the inlay channel cross section $A_{\text{q,InlayChannel}}$ which can be directly expressed in dependency of the channel height c as

$$A_{\text{q,InlayChannel}} = n \cdot b_{MI} \cdot c = k \cdot b \cdot c. \tag{29}$$

Experiments have been performed in analogy to the description in Section II-E with different inlay geometries for ($n = 6/k = 0.31/c = 0.2$ mm, $c = 1.25$ mm, $c = 2$ mm, $c = 3$ mm) and ($n = 12/k = 0.63/c = 0.2$ mm, $c = 1.25$ mm, $c = 2$ mm, $c = 3$ mm). The measurement results presented in Fig. 13 show a good matching with the theoretical calculations (agreement within 20% over a wide range of c). The pressure drop in the internal cooling structure and the thermal resistance in the channel's inlet/outlet area are based on experimentally derived coefficients (as discussed in Section II-D-1 and II-D-2) which contributes to the good accuracy of the results.

IV. Direct Water Cooling Versus Conventional Air-Cooling

The experimentally measured thermal resistances for optimized cooling geometries are $R_{\text{th,SlotChannel}} \approx 0.12$ K/W (Fig. 7) and $R_{\text{th,Inlay}} \approx 0.10$ K/W (Fig. 13). Again, we would like to point out that this is the thermal resistance between the module base plate and the water ambient temperature. For thermal losses of 150 W and an ambient (cooling water) temperature of $T_{\text{a,H20}} = 80\,^{\circ}$C the power module base plate therefore will be on an average temperature of $T_{\text{BasePlate,Inlay}} = 80 + 150 \cdot 0.10 = 95\,^{\circ}$C.

Designing a conventional heat sink with forced convection cooling that guarantees a power module base plate temperature of 95 °C under these assumptions would be a difficult task. The main problem is that the power module under consideration has a comparably small base plate of 8.5 cm^2 resulting in a thermal power flow of more than 17 W/cm^2. This creates a hot spot on the heat sink surface due to the limited thermal conductivity of the metal and, therefore, only a small portion of the heat sink surface can be effectively used for heat spreading.

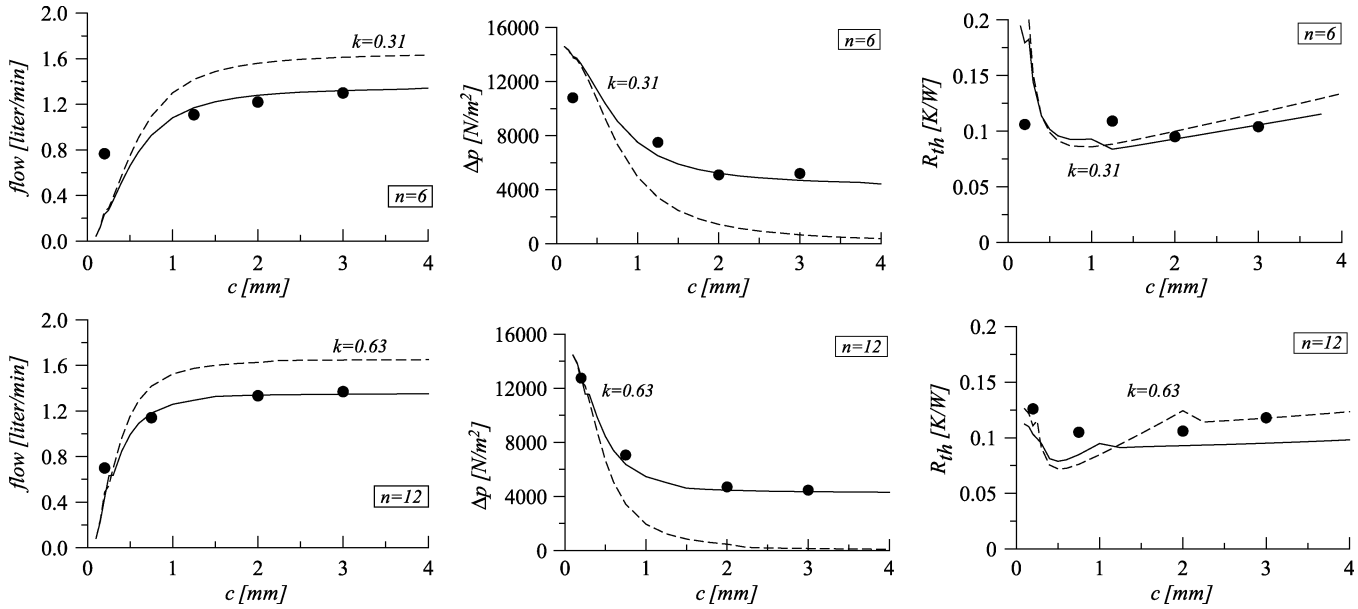

Fig. 13. Neglecting the influence of the pipe structure inside the heat sink results in the characteristics shown by dashed lines (already shown in Fig. 10 and Fig. 12). Performing the calculations as described in Section II-D gives the curves shown by solid lines. The black dots indicate results of experimental measurements. For $n = 6$ a structure characterized by $k = b_{MI}/(b/n) = 1.0\ \text{mm}/(19.2\ \text{mm}/6) = 0.31$ has been manufactured; for $n = 12$ we used $k = b_{MI}/(b/n) = 1.0\ \text{mm}/(19.2\ \text{mm}/12) = 0.63$.

Extruded profile cooling aggregates show low manufacturing costs but are characterized by thermal resistance values typically larger than 1.0 K/W; in the case at hand this would result in a module base plate temperature over 230 °C. In order to achieve a thermal resistance well below 1.0 K/W a sophisticated hollow-fin cooling aggregate with fin geometries optimized in terms of flow resistance and thermal efficiency and a powerful fan would have to be employed. Fro example, the hollow fin cooling aggregate "Fischer Elektronik LA V 14" ($120 \times 120 \times 200\ \text{mm}^3$) [15] in combination with a fan "Papst 4184 NXH" (24 V, 11 W, 237 m^3/h, $119 \times 119 \times 38\ \text{mm}^3$) [16] shows, according to the datasheet, an average thermal resistance of $R_{th} \approx 0.06$ K/W (configuration shown in Fig. 14). However, numerical simulations with ICEPAK showed that this is only valid for a thermal power flow distributed over the whole heat sink top plate (240 cm^2, power flow density of about 0.63 W/cm^2). Therefore, employing a power module with a base plate surface of only 8.5 cm^2 creates a hot spot in the vicinity of the module resulting in $R_{th} \approx 0.14$ K/W.

In conventional configurations one has to add a layer of thermal grease for avoiding air gaps of high thermal resistance between heat sink surface and power module base plate resulting in an additional resistance of $R_{\text{th,ThermalGrease}} \approx 0.07$ K/W (as derived from a datasheet of the same power module package [17] as employed in this study). The total thermal resistance of 0.21 K/W would result in a module base plate temperature of about 111.5 °C representing a 110% increase of the temperature drop within the cooling system. If the thermal interface would be realized with special foil products (e.g., [18]) instead of thermal grease the total thermal resistance could be reduced significantly. The thermal resistance of the foil "KU-CB 2000" [18] characterized by $R_{\text{th,Foil}} \approx 0.01$ K/W could result in a total thermal resistance of 0.15 K/W and a base plate temperature of 102.5 °C. In summary, the air cooling would increase the cooling-system temperature drop by 50% compared to direct water cooling.

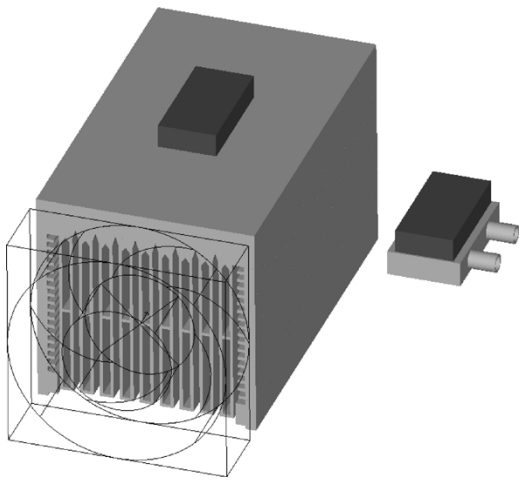

Fig. 14. Air-cooled aluminum heat sink (hollow fin cooling aggregate) with carbon foil thermal interface between heat sink and power module on top providing $R_{th} \approx 0.15$ K/W as compared to the power module mounted on the direct water cooler with $R_{\text{th,Inlay}} \approx 0.10$ K/W. The volumes of the cooling systems (without power modules) are 3500 cm^3 and 37 cm^3, respectively. The fan would consume 11 W while the water pump consumes 7 W of electrical power.

As shown in Fig. 14 the volume of the direct water cooling system is only about 1% of the volume of the conventional forced convection air-cooled system. For a fair comparison one must not forget that the water cooling system also employs a pump, pipes and a heat exchanger which is not shown in Fig. 14.

The main problem with air cooling in this example is that it is nearly impossible to reduce the thermal resistance (ambient to power module base plate) significantly below 0.15 K/W in

case conventional heat sink materials like aluminum and conventional fans are employed. According to a simulation, manufacturing the heat sink from copper [$\lambda_{th,Cu} = 390$ W/(Km)] instead of aluminum [$\lambda_{th,Al} = 210$ W/(Km)] would result in a total thermal resistance (including the carbon foil) of 0.10 K/W but would not be a practical choice for mass production. In this paper, we determined $R_{\mathrm{th,WaterCooling}} \approx 0.10$ K/W, but with use of a higher power pump a significant reduction of this value would easily be possible. Another general advantage of water cooling is the greater flexibility for the converter design. In case of air cooling, the air flow should not be hindered because this would significantly reduce the efficiency resulting in an increase of the thermal resistance. With water cooling the heat is transported away from the power modules via pipes and transferred to the ambient by a heat exchanger at a different place.

V. Cooling Multichip Modules

All theory presented so far is based on the assumption of an equal distribution of the thermal power flow over the base plate area. Also the experiments have been performed under this assumption by employing a copper block acting as a very efficient heat spreader and guiding the heat from the heating resistors directly to the base plate. The R_{th}-values presented in Fig. 7 and Fig. 13 must be interpreted under this assumption. If a small chip with area $A_{\mathrm{CHIP}} < A_{\mathrm{BasePlate}}$ is positioned inside the power module, the actual thermal resistance has to be calculated in general form as

$$R_{\mathrm{th,CHIP,Junct-ambient}} = R_{\mathrm{th,CHIP,Junct-BasePlate}} + R_{th}(c) \cdot \frac{A_{\mathrm{BasePlate}}}{A_{\mathrm{CHIP}}} \cdot f^{-1}_{\mathrm{HeatSpreading}} \quad (30)$$

where $R_{th}(c)$ is the value given in Fig. 7 for the slot channel or Fig. 13 for the inlay channel. Heat spreading (characterized by a problem-specific factor $f_{\mathrm{HeatSpreading}} > 1$) will increase the cross-sectional area available for heat flow and therefore reduce the thermal resistance. If a chip inside the power module is molded onto a DCB where the DCB bottom copper layer is the module's base plate, heat spreading might be small ($f_{\mathrm{HeatSpreading}} \approx 1$) and the total thermal resistance of this chip is large according to (30) especially if the chip is of small size. Employing the inlay concept the total thermal resistance will be reduced because the metallic inlay itself will contribute to heat spreading. If the power module's base plate is made of a thick copper plate (2...3 mm) the copper plate will perform the heat spreading and a slot channel scheme might be sufficient.

VI. Conclusion

This paper presents a method for the calculation of the thermal resistance between the base plate of a power module and the ambient for direct water cooling with analytical equations based on correlations with empirical data and, to a certain extent, curve fitting of numerical solutions. All equations shown in this paper have been combined into a Mathematica [19] script which allows the immediate calculation of thermal resistance values for various geometries. Performing numerical simulations instead would be extremely time-consuming and therefore not practical. Experimental results have shown a high accuracy of the theory.

Considering the characteristic of the pump is essential to find the optimum geometry that minimizes the thermal resistance. A simple slot channel concept shows very good results. Employing a novel inlay scheme as proposed in the paper reduces the thermal resistance and improves the heat spreading in case of a multichip power module. The pump discussed in the paper accomplishes a pressure of about 80 mbar and a water flow of 1.2 l/min which gives for the optimized inlay channel scheme a thermal resistance $R_{\mathrm{th,BasePlate-ambient}}$ of less than 0.85 K/W per cm^2 (0.10 K/W for a 2.5 cm $\times$ 3.4 cm base plate) [20], [21].

References

[1] J. W. Kolar and F. C. Zach, "A novel three-phase utility interface minimizing line current harmonics of high-power telecommunications rectifier modules," in *Proc. 16th IEEE Int. Telecommunications Energy Conf.*, Vancouver, BC, Canada, Oct. 30–Nov. 3 1994, pp. 367–374.

[2] U. Drofenik and J. W. Kolar, "Thermal analysis of a multichip Si/SiC-power module for realization of a bridge leg of a 10 kW Vienna rectifier," in *Proc. 25th IEEE Int. Telecommunications Energy Conf.*, Yokohama, Japan, Oct. 19–23, 2003, pp. 826–833.

[3] Eheim, Inc. Centrifugal Pump 1048. [Online] Available: http://www.eheim.com/

[4] J. H. Spurk, *Strömungslehre—Einführung in die Theorie der Strömungen*, 4th ed. Berlin, Germany: Springer-Verlag, 1996.

[5] H. D. Baehr and K. Stephan, *Wärme- und Stoffübertragung*, 3rd ed. Berlin, Germany: Springer-Verlag, 1998.

[6] V. Gnielinski, "Berechnung mittlerer Wärme- und Stoffübertragungskoeffizienten an laminar und turbulent überströmten Einzelkörpern mit Hilfe einer einheitlichen Gleichung (in German)," *Forsch. Ing. Wes. 41*, pp. 145–153, 1975.

[7] A. Zukauskas and J. Ziugzda, "Heat transfer in laminar flow of fluid," in *Thermohpysics 2, Academy of Science of the Lithuanian SSR*. Vilnius, Russia: Institute of Physics and Technical Problems of Energetics, 1973.

[8] D. B. Tuckermann and R. F. W. Pease, "High-performance heat sinking for VLSI," *IEEE Electron. Device Lett.*, vol. EDL-2, no. 5, pp. 126–129, May 1981.

[9] W. Beitz and K.-H. Grote, *Dubbel—Taschenbuch für den Maschinenbau*, 20th ed. Berlin, Germany: Springer-Verlag, 2001.

[10] Fluke, Inc. 80 BK Integrated DMM Temperature Probe. [Online] Available: http://www.fluke.ch/

[11] Fluent, Inc. 3D-CFD FEM Software ICEPAK. [Online] Available: http://www.icepak.com

[12] Fujikura, Inc. Pre-Amplified, Pre-Calibrated and Pre-Compensated Pressure Sensor XFDM-025KPDSR. [Online] Available: http://www.fujikura.co.uk/pdf/xfdm.pdf

[13] Remag, Inc. Flow Sensor Vision 2000. [Online] Available: http://www.remag.ch/vision2000/_eng/default.htm

[14] V. Gnielinski, "New equations for heat and mass transfer in turbulent pipe and channel flow," *Int. Chem. Eng.*, vol. 16, no. 2, pp. 359–367, Apr. 1976.

[15] Fischer Elektronik GmbH. Hollow-Fin Cooling Aggregates With Air-Flow Chamber LA V 14. [Online] Available: http://www.fischerelektronik.de

[16] ebm-papst Germany. DC-Axiallüfter, Serie 4100N, Typ 4184 NXH, $119 \times 119 \times 38$. [Online] Available: http://ww.papst.de

[17] IXYS Corporation. Package of Power Module VUI 30-12 N1. [Online] Available: http://www.ixys.com

[18] Kunze Folien GmbH. Graphite Interface Material KU-CB 2000. [Online] Available: http://www.heatmanagement.com

[19] Wolfram Research. Software Mathematica. [Online]Available: http://www.wolfram.com/

[20] Y. Murakami and B. B. Mikic, "Parametric optimization of multichanneled heat sinks for VLSI chip cooling," *IEEE Trans. Compon. Packag. Technol.*, vol. 24, no. 1, pp. 2–9, Mar. 2001.

[21] I. Mudawar, "Assesment of high-heat-flux thermal management schemes," *IEEE Trans. Compon. Packag. Technol.*, vol. 24, no. 1, pp. 122–141, Mar. 2001.

Uwe Drofenik (S'96–M'00) was born in Modeling, Austria, in 1970. He received the M.Sc. degree (with honors) and the Ph.D. degree (with honors) in electrical engineering from the Vienna University of Technology, Austria, in 1995 and 1999, respectively.

He is currently performing scientific research and teaching at the Swiss Federal Institute of Technology Zurich where he is developing web-based interactive educational software. During 1996, he was a Researcher at the Masada-Ohsaki Laboratory, University of Tokyo, Japan. His research interests include thermal analysis of power systems, power factor correction, single- and three-phase converters, numerical simulation, and Java programming. He has published 34 conference papers, five journal papers, and four patents.

Dr. Drofenik is Member of the Austrian Society of Electrical Engineering (OVE).

Gerold Laimer (S'02) was born in Salzburg, Austria, on January 16, 1971. He received the M.Sc. degree (with honors) in electrical engineering from the University of Technology Vienna, Vienna, Austria, in 1999 and is currently pursuing the Ph.D. degree at the Power Electronic Systems Laboratory, ETH Zurich.

In May 1999, he was with Elin EBG Electronic, Vienna, working on control hardware and switched mode power supplies for frequency inverters. His current research is focused on ultra compact ac–dc three phase PWM (Vienna) rectifier based on SiC technology.

Mr. Laimer is a Member of the Austrian Society of Electrical Engineering (OVE).

Johann W. Kolar (M'89–SM'04) received the Ph.D. degree (with highest honors) in industrial electronics from the University of Technology Vienna, Vienna, Austria, in 1984.

From 1984 to 2001, he was with the University of Technology in Vienna, where he was teaching and working in research in close collaboration with the industry in the fields of high performance drives, high frequency inverter systems for process technology and uninterruptible power supplies. He has proposed numerous novel converter topologies, e.g., the VIENNA rectifier and the three-phase ac–ac sparse matrix converter concept. He has published over 200 scientific papers in international journals and conference proceedings and has filed more than 50 patents. He was appointed Professor and Head of the Power Electronics Systems Laboratory, Swiss Federal Institute of Technology (ETH) Zurich, in 2001. The focus of his current research is on novel ac–ac and ac–dc converter topologies with low effects on the mains for telecommunication systems, more-electric-aircraft applications, and distributed power systems utilizing fuel cells. A further main area of research is the realization of ultra-compact intelligent converter modules employing latest power semiconductor technology (SiC) and novel concepts for cooling and EMI filtering.

Dr. Kolar is a member of the IEEJ. From 1997 through 2000, he was an Associate Editor of the IEEE TRANSACTIONS ON INDUSTRIAL ELECTRONICS and since 2001 was an Associate Editor of the IEEE TRANSACTIONS ON POWER ELECTRONICS. He is a Member of Technical Program Committees of numerous international conferences in the field (e.g., Director of the Power Quality branch of the International Conference on Power Conversion and Intelligent Motion).